Batteries & Supercaps

Research Article
doi.org/10.1002/batt.202400451

Chemistry Europe
European Chemical Societies Publishing

www.batteries-supercaps.org

NiFe-NO_3 Layered Double Hydroxide as a Novel Anode for Sodium Ion Batteries

Marco Fortunato,*[a, b] Angelina Sarapulova,[c, d, e] Björn Schwarz,[e] Anna Maria Cardinale,[a] and Sonia Dsoke[c, d, e, f]

2D materials are emerging materials for energy storage and among these layered double hydroxides (LDHs) seem particularly promising due to their structure, easily adjustable composition, and cheapness. This study marks the first reported application of an LDH, specifically NiFe-NO_3 LDH, as conversion anode material in a sodium half-cell, to the best of our knowledge. Despite an initial loss in capacity, the material demonstrates notable stability, retains a high specific capacity even after 50 discharge/charge cycles (~500 mAh/g). The intricate reaction mechanism was explored using various *ex-situ* techniques such as DC magnetometry and FTIR, as well as *in-operando* X-ray Absorption Spectroscopy (XAS). The proposed Na-storage mechanism in NiFe-NO_3 LDH involves an initial irreversible "activation" during the first sodiation, characterized by a phase change reaction that leads to the formation of NiO_x and Fe_3O_4, followed by a reversible mechanism involving both intercalation and conversion in subsequent cycles.

Introduction

In the last years, the increasing competitiveness of renewable energy sources with fossil fuels has driven a great acceleration to the sustainable energy transition and to electrification, but additional efforts have yet to be done. As an example, the electric current transmission and distribution can be improved by grid energy storage, making the energy market more efficient, cheaper, and more competitive.[1,2]

Batteries are currently the best solution for medium energy storage concerning life cycle and storage cost. However, high investment, shortage of raw materials and their environmental impact have weakened their position as a grid storage technology.[3] Moreover, commercial Li-ion batteries (LIB) (the most widespread rechargeable batteries) reach their physico-chemical limits in terms of energy density.[4] Hence, LIB technology must be upgraded (advanced LIB) or modified in its core elements, considering abundance, environmental friendliness, and safety.[5]

Nowadays, one of the most promising solutions for these issues is the replacement of lithium with sodium, mainly for grid storage where huge amounts of materials are needed. Sodium is one of the most abundant elements of the earth's crust, with a reduction standard potential of −2,71 V. In recent years, lots of promising different anode materials have been developed for sodium-ion batteries (SIBs) to achieve a sufficient level of cycling life, safety, and energy density.

Until now, only a few have reached a technological level to achieve marketing, such as Prussian blue analogue (PBA) patented by NATRON and the polyanionic compounds-based batteries commercialised by TIAMAT.[6,7] Numerous start-ups are presently engaged in the development of hard carbon materials, regarded as one of the most promising options for anodes. However, their commercial viability is hindered by challenges such as low coulombic efficiency in the initial cycle and high surface area, resulting in adverse side reactions and substantial consumption of electrolyte for solid electrolyte interface formation (SEI).[8,9]

Furthermore, those kinds of materials need to be produced under critical high-temperature conditions, linked with expensive treatment that could limit their large-scale application.[8,10]

Two-dimensional materials (2D) are acquiring increasing interest in the field of electrochemical energy storage and conversion. They can offer a high intercalation surface and provide short distances for Na^+ migration, making this group of compounds very attractive for SIBs.[4]

In the framework of the 2D materials, the layered double hydroxides (LDHs) seem to be excellent candidates for these

[a] M. Fortunato, A. M. Cardinale
Dipartimento di Chimica e Chimica Industriale, Università di Genova Via Dodecaneso 31, 16146 Genova, Italy

[b] M. Fortunato
Institute of Condensed Matter Chemistry and Technologies for Energy, CNR, Via de Marini 6, 16149 Genoa, Italy
E-mail: marco.fortunato@cnr.it

[c] A. Sarapulova, S. Dsoke
Fraunhofer Institute for Solar Energy Systems, Dep. Electrical Energy Storage, Heidenhofstr. 2, 79110 Freiburg, Germany

[d] A. Sarapulova, S. Dsoke
Freiburg Materials Research Center (FMF), Stefan-Meier-Straße 21, 79104 Freiburg, Germany

[e] A. Sarapulova, B. Schwarz, S. Dsoke
Institute for Applied Materials -Karlsruhe Institute of Technology, Hermann-von-Helmholtz-Platz1,76344 Eggenstein Leopoldshafen, Germany

[f] S. Dsoke
Albert Ludwig University Freiburg, Department of Sustainable Systems Engineering (INATECH), Emmy-Noether-Straße 2, 79110, Freiburg, Germany

Supporting information for this article is available on the WWW under https://doi.org/10.1002/batt.202400451

Research Article
doi.org/10.1002/batt.202400451
Chemistry Europe
European Chemical Societies Publishing

purposes thanks to their chemical composition and their peculiar characteristics.

The LDHs are a family of compounds constituted by an hydrotalcite-like structure with the general formula:

$$[M_{1-x}N_x\ (OH)_2]^{x+}(A^{n-})_{x/n} \cdot mH_2O],$$

where M and N are, respectively, a divalent and trivalent metal, and x is the ratio N/(N + M) that can be theoretically tuned (usually $0.20 \leq x \leq 0.33$).[11–13]

A^{n-} is an anion with n^- charge that can be chosen among a broad range of both, organic and inorganic components, and all the constituting elements could be appropriately selected to build up a compound suitable for different specific usage, so are widely employed as anion exchanger and adsorbent finding application also in the field of catalysis.[14–16] In recent years, LDHs have also been applied as active materials in supercapacitors.[17–20] Furthermore, they also find applications in the field of batteries.[21–23] For example, Li et al.[24] tested NiAl-NO_3 LDH as an anode material for LIB, showing good stability and specific capacity (697 mAh/g after 400 cycles with an applied current of 0.5 A/g), but until now, the literature about LDHs as materials for SIBs is lacking.

In this work, we report for the first time the application of NiFe-NO_3 LDH as a conversion anodic material in SIBs, it presents in its structure two metals that could be electrochemical centres and could lead to a theoretical capacity of 477 mAh/g higher than the 300/350 mAh/g of commercial hard carbon, furthermore the compound was synthetised via one pot coprecipitation at low temperature a simple, economically, easily scalable and green process in comparison with the high temperature calcinations needed for hard carbon.[24]

The material was than comprehensively characterized by means of **Inductively Coupled Plasma – Optical Emission Spectroscopy** (ICP-OES), powder x-ray diffraction (PXRD), Fourier transform infrared spectroscopy (FTIR) and field emission scanning electron microscopy (FE-SEM). The obtained material was then used to prepare electrodes for the electrochemical tests, showing a relatively good stability and a high specific capacity. The reaction mechanism in sodiation/desodiation was deeply investigated through *ex-situ* (magnetic measurements) and *in-operando* analysis (X ray adsorption spectroscopy) revealing a mixed conversion/intercalation reaction.

Results and Discussion

Physio-Chemical Characterization

The ratio between the metals was confirmed to be 2:1 by ICP-OES analysis, as shown in Table 1.

The FT-IR spectrum (figure 1) shows only a few signals; the broad and deep band centred at 3400 cm^{-1} is due to the O–H stretching of the hydroxides and intercalated water molecules, the signal of medium intensity at 1640 cm^{-1} is attributable to the bending mode of water and finally an absorption at 1380 cm^{-1} is related to the υ3vibration of nitrate.[22]

Table 1. amount of Ni and Fe in the LDH sample resulting from ICP-OES analysis.

	Quantity (mass %)	Quantity (moles)	Atomic ratio
Ni	17	0.30	1.00
Fe	35.8	0.61	2.00

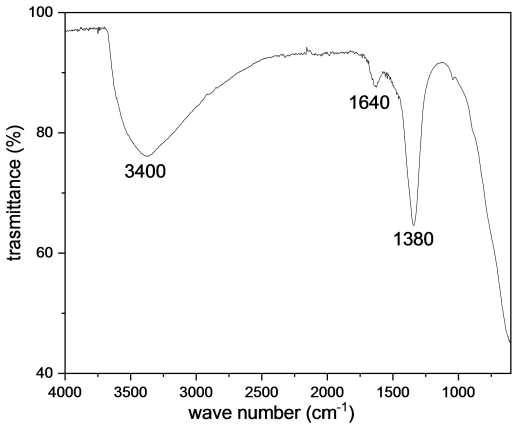

Figure 1. FT-IR spectra of NiFe-NO_3 LDH.

The diffraction pattern of NiFe-NO_3 LDH (figure 2) confirms that the structure is the typical hexagonal LDHs one (space group R −3 m),[25] and the cell parameters obtained by means of WinPLOTR suite[26] are: a = 3. 08(0) Å and c = 23.4(9) Å. All the reflections are broad, underlining the small crystallite size and the low crystallinity of the compound, and they are divided in symmetric 003; 006; 009; 110; 113 and asymmetric 012; 015; 018.[12,19,25,27,28] These last one are typical of turbostratic compounds where the different basal planes have slipped out of alignment.

That characteristic is also apparent from the FE-SEM images at low magnification (Figure 3) where basal crystallographic lattice planes of material are stacked in a random orientation.

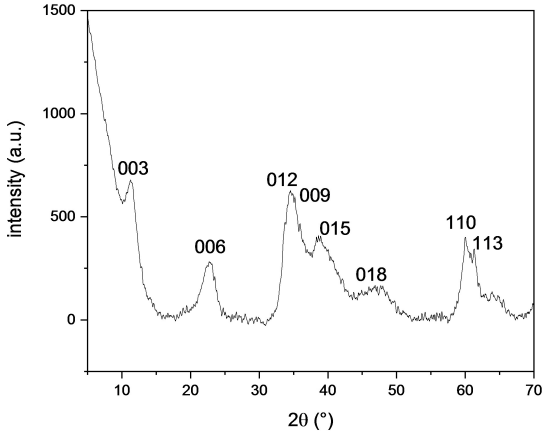

Figure 2. PXRD pattern of NiFe-NO_3 LDH.

Research Article
doi.org/10.1002/batt.202400451
Chemistry Europe
European Chemical Societies Publishing

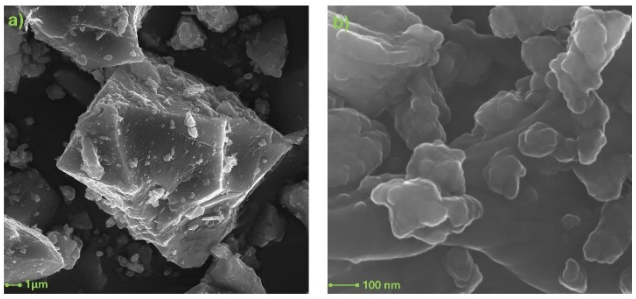

Figure 3. FE-SEM images at low a) and high b) magnification of NiFe-NO_3 LDH.

Furthermore, in the picture at high magnification (Figure 3b) the nano structuring of the material surface could be seen.

As reported in previous work all the NO_3^- lays at the interlayer and the amount of the surface absorbed is negligible.[29]

According to the previous analysis and the thermogravimetric curve (supplementary material, figure S1) the formula is confirmed to be $[Ni_{0,66}Fe_{0,33}(OH)_2]\ (NO_3)_{0,33}\cdot H_2O$.

Electrochemical Studies: NiFe-NO_3 LDH in Sodium Metal Half Cell

A cyclic voltammogram (CV) of the LDH electrode in the half cell configuration vs. Sodium metal counter electrode was performed in the potential range 0.01–3 V vs. Na^+/Na. The experiment was carried out at increasing scan rates between 0,1 and 10 mV/s (3 cycles of sodiation/desodiation for each) at 20 °C. In Figure 4a, the initial three cycles at a low scan rate reveal a subtle peak at 0.97 V during the first sodiation, attributed to electrolyte degradation and the formation of a solid electrolyte interface (SEI). Progressing towards lower potentials, a broad asymmetric peak at 0.43 V emerges, associated with the irreversible reaction. Both these peaks vanish in subsequent cycles, replaced by prominent peaks at 0.75 V and 0.55 V due to a partial reduction of Fe^{3+} and Ni^{2+}. During desodiation, two major peaks at 0.75 V and 1.45 V are present and are retained also in the subsequent cycles, they are attributable to the reoxidation of metals.[30,31]

Upon increasing the scan rate (Figure 4d), the electrode experiences polarization, but the peaks remain evident.

Those experimental data were also used to calculate the percentage of contribution to the total specific capacity of the outer and inner process with the Trasatti method, demonstrating that the involved reactions are mainly driven by diffusion but there is also a ~15 % of surface-controlled contribution (Figure S2).

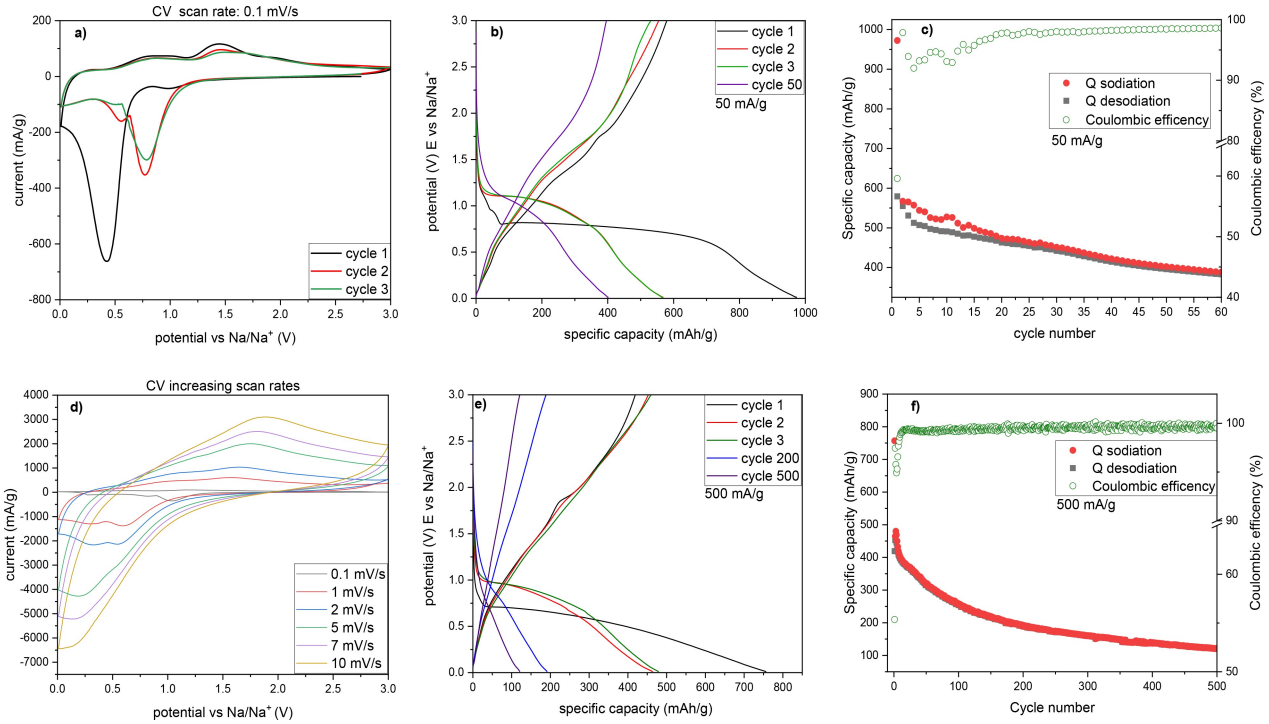

Figure 4. electrochemical characterization of NiFe-NO_3 LDH based half-cells: CV plot, current vs potential first three cycles at 0,1 mV/s scan rate a). GCPL curves, potential vs specific capacity b) specific capacity and coulombic efficiency vs cycle number c) with an applied current of 50 mAg^{-1}. Second cycle for each scan rate from 0,1 to 10 mV/s d). Potential vs specific capacity e) specific capacity and coulombic efficiency vs cycle number f) with an applied current of 500 mAg^{-1}. The electrolyte used is 1 M $NaClO_4$ solution dissolved in a mixture of 1 : 1 ethylene carbonate (EC) and dimethyl carbonate (DMC) with a 5 % of fluoroethylene carbonate (FEC).

Research Article
doi.org/10.1002/batt.202400451
Chemistry Europe
European Chemical Societies Publishing

Figure 4b depicts the galvanostatic curve of the NiFe-NO_3 LDH electrode under a 50 mA/g applied current. In the first reduction, a shoulder appears around 1 V, followed by a long-tilted plateau spanning from 0.8 V to 0.6 V, it is succeeded and partially overlapped by another contribution ending at 0.2 V, all those observations are consistent with what was presented in the CV plot. After the first cycle, all contributions are replaced by a signal composed of platform and slope contributions. During desodiation, two main contributions are evident, persisting in subsequent cycles, aligning with the previously discussed CV data.

In the initial sodiation, the specific capacity reaches 972 mAh/g. However, during the first desodiation, only 579 mAh/g is delivered, resulting in a coulombic efficiency of 60% (see Figure 4c). This may be attributed to irreversible reactions associated with partial electrolyte degradation, solid electrolyte interface (SEI) formation, and material irreversible modification. As cycles progress, the coulombic efficiency significantly improves, exceeding 95%. After 60 discharge/charge cycles, the material maintains a capacity of 388 mAh/g during sodiation, indicating a quite stable SEI and moderate cyclability.

To strengthen this hypothesis of stabilization after the first cycles was performed a (dQ/dV) vs V analysis at the 3rd and 50th cycle (Figure S3) demonstrating that, even if the capacity drops the position of the peaks relative to electrochemical reactions is retained.

Furthermore, a galvanostatic cycling within the same potential range at 500 mA/g for 500 cycles was conducted (Figure 4e). The initial specific capacity in sodiation is 760 mAh/g, contrasting with 420 mAh/g in desodiation. The initial coulombic efficiency is 55%, but it notably increases in subsequent cycles, stabilizing at approximately 98% (see Figure 4f). After 500 discharge/charge cycles, the material retains only 122 mAh/g underlining some stability issue.

To delve deeper into the material's response at high current an examination of rate capability (RC) was undertaken, involving a gradual increase in current from 50 mA/g to 10 A/g (see Figure 5). The initial 5 cycles (at 50 mA/g) closely mirror those observed in the GCPL under identical conditions with an initial specific capacity of 945 mAh/g in sodiation and an irreversible capacity loss in the first desodiation, with a 60% retention of specific capacity. In next cycles the capacity retention increases and after the fifth cycle the material delivers 475 mAh/g.

With an increase in the applied current, the initial specific capacity experiences a decline, maintaining a relatively stable trend over the five cycles, characterized by a "stair-like" pattern. At an applied current of 10 A/g, the electrode can only deliver 45 mAh/g. Nonetheless, NiFe-NO_3 LDH demonstrates that reverting to the initial applied current of 50 mA/g could yield a reversible capacity of 430 mAh/g., lower but still comparable to the one registered after the fifth cycle.

The material was found to lack sufficient stability to meet the requirements for a commercial anode, such as hard carbon. However, it represents a potential alternative and marks a step forward compared to similar $Ni(OH)_2$-based compounds, which typically deliver less than 150 mAh/g after 50 cycles.[32]

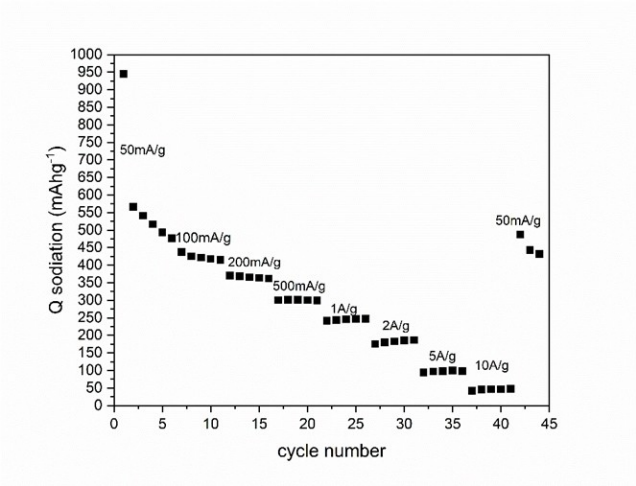

Figure 5. RC plot of NiFe-NO_3 LDH at increasing applied currents, from 50 mA/g to 10 A/g. The electrolyte used is 1 M $NaClO_4$ solution dissolved in a mixture of 1 : 1 ethylene carbonate (EC) and dimethyl carbonate (DMC) with a 5% of fluoroethylene carbonate (FEC).

The analyses conducted thus far have proven insufficient in providing comprehensive information about the reaction mechanism. Therefore, a more thorough study involving various techniques were additionally performed. The electrodes were investigated *ex situ* before the electrochemical test and after the

initial sodiation and desodiation. The first technique used was PXRD but it didn't gave back much information, all the three samples present a disturbed long range order and only in the pristine material are present few recognisable peaks attributable to the LDH (figure S4). Since different Ni and Fe compounds have a typical magnetic behaviour, the electrodes were also subjected to magnetic measurements. Additionally, to gain insights into the oxidation state of the elements and to understand the role of each metal, an *in-operando* X-ray absorption analysis was also performed.

Magnetic Property Studies

Magnetic properties contain valuable information about the transition metals' oxidation states, their local coordination symmetry, their spatial distribution and much more.

As illustrated in figure S5, supplementary materials, the zero-field-cooled (ZFC) and field-cooled (FC) susceptibility χ curves (acquired at 500 Oe and 5 kOe, respectively) overlap with each other from 300 down to approximately 30 K. The inverse dependence of susceptibility on temperature points to a Curie-Weiss behaviour that is characteristic for localized magnetic moments. Below approximately 30 K, the susceptibility values measured at 5 kOe fall below those measured at 500 Oe, indicating a departure from a pure paramagnetic behaviour with a linear dependence of magnetization on the magnetic field. Distinct bifurcations of the ZFC and FC curves emerge, with the FC curves reaching a maximum at 9.0(5) K (500 Oe)

Research Article
doi.org/10.1002/batt.202400451
Chemistry Europe
European Chemical Societies Publishing

and 6.0(5) K (5 kOe), indicating the realization of a ferro-/ferrimagnetic ordering at these low temperatures.

The χT vs. T plot shown in Figure 6 (derived from the FC curve at 5 kOe), reveals that the high temperature magnetic properties above approximately 50 K deviate slightly from a pure Curie-Weiss behaviour that would lead to a constant χT value over temperature. However, the "average" measured χT value in this temperature range agrees well with the assumption that Ni and Fe are present as Ni^{2+} and Fe^{3+} in the pristine NiFe-NO_3 LDH. Ni^{2+} has the electronic configuration [Ar]3d^8 with spin $S=1$ in octahedral coordination with a paramagnetic spin-only moment of 2.83 μ_B and Fe^{3+} has the electronic configurations [Ar]3d^5 with spin $S=5/2$ (high-spin) in octrahedral coordination and a paramagnetic spin-only moment of 5.92 μ_B. With the presence of 0.66 Ni^{2+} and 0.33 Fe^{3+} per formula unit, the calculated total effective paramagnetic moment is 4.12 μ_B, corresponding to a Curie constant of $C_{calc}=2.126\ cm^3\,K\,mol^{-1}$ (see supplementary information for details). The proximity of this calculated value to the $\chi T=C$ value at high temperatures (figure 6) confirms that Ni in NiFe-NO_3 LDH is present as Ni^{2+} and Fe is present as Fe^{3+}. The increasing χT with decreasing temperature suggests the presence of slight magnetic ordering even at elevated temperatures, deviating from a strictly constant Curie constant. All this information aligns well with literature,[33] indicating that the material can be considered pure.

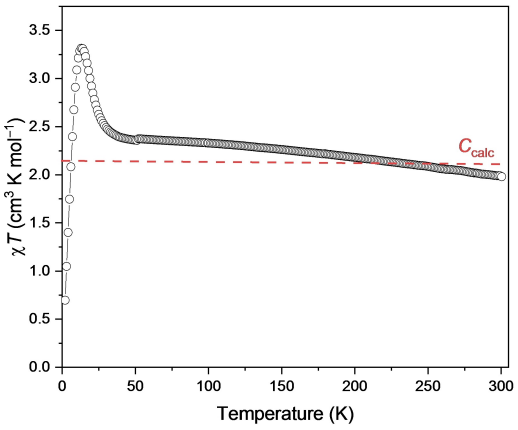

Figure 6. χT vs. temperature plot as obtained from the FC susceptibility curve measured at 5 kOe. The Curie constant C_{calc} as obtained if the Ni and the Fe would be present as Ni^{2+} and Fe^{3+} in NiFe-NO_3 LDH is inserted as dashed line.

The carbon and binder additives in the electrode material do only contribute with a negligible small diamagnetic signal. As shown in Figure S6 in supplementary materials, the field scans of the pristine powder and the electrode with pristine powder coincide to good approximation when considering only the mass of the active material in the electrode. Therefore, for the electrode materials only the mass of the active material has been considered for the evaluation.

The field scans for the pristine, discharged, and recharged NiFe-NO_3 LDH electrode material differ from one another significantly.

As shown in Figure 7, the field scans for the pristine material align with the susceptibility measurements discussed above. At 300 K, a pure linear magnetic moment-field behaviour, characteristic of a Langevin paramagnet with localized moments, is evident. At 2 K, the presence of magnetic order is confirmed by the observed hysteresis. The ferrimagnetic order, inferred from the bifurcation temperature of the ZFC/FC with an increasing measuring field, also corresponds to the non-saturating behaviour, even at 7 Tesla.

In contrast, the discharged sample predominantly exhibits a field scan typical of a soft ferro/ferrimagnetic material, reaching a saturation magnetization of approximately 0.25 μ_B per formula unit at around 1 T at 300 K. The slight decrease in magnetization with an increasing field demonstrate that diamagnetic contributions from closed shell electrons and from the carbon black also play a (minor) role in the overall signal. In a hypothetical ferromagnetic phase with all Ni^{2+} (spin $S=1$) and Fe^{3+} (spin $S=5/2$) aligned in parallel, a total ordered moment of about 3 μ_B would be expected (see supplementary information for details). The observed saturation magnetization of only about 0.25 μ_B therefore rather points to the formation of some sort of a (Ni,Fe)-oxide with ferrimagnetic order where individual magnetic moments compensate each other to large extend and only a comparably small spontaneous net magnetization is

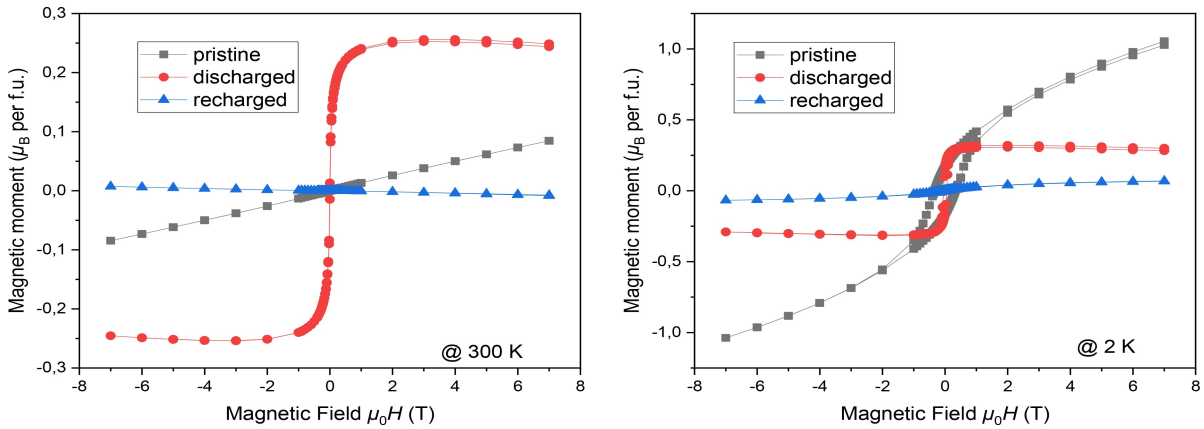

Figure 7. Magnetic moment vs. field plots for the pristine, discharged, and recharged NiFe-NO_3 LDH as obtained from the electode composite materials measured at a) 300 K and b) 2 K.

Research Article
doi.org/10.1002/batt.202400451
Chemistry Europe
European Chemical Societies Publishing

realized instead.[34] A more specific phase assignment cannot be provided here, since a nickel spinel ferrite, for instance, with a Ni:Fe ratio of 2:1 has not been reported yet.[34] The fact that the same saturation magnetization has been measured at 2 and at 300 K indicates that the ordering temperature of this ferromagnetic compound is well above 300 K. For the re-charged sample, the absolute values of magnetization are strongly reduced in general compared to the values of the pristine and the discharged sample. The magnetization slightly decreases with an increasing field at 300 K, indicating even a dominant diamagnetic contribution. This could be explained by an antiferromagnetic ordering of the Ni respectively Fe moments that cancel out each other. An antiferromagentic ordering has also been reported for NiO and nanosized α-Fe_2O_3[35,36] for instance, and it can be speculated that a corresponding antiferromagentic (Ni,Fe)O respectively a nanosized α-$(Ni,Fe)_2O_3$ phase might have formed here.

In-Situ X-ray Absorption Spectroscopy (XAS)

The NiFe-NO_3 LDH based electrode was also subjected to *operando* XAS analysis at the Hamburg synchrotron (DESY) to clarify its reaction mechanism. The XANES (X-ray Absorption Near Edge Structure) spectra of the pristine NiFe-NO_3 LDH compound reveal that the Ni and Fe oxidation states are 2+ and 3+, corresponding to the K-edge position of standard oxides. In sodiation, Fe^{3+} undergoes reduction to Fe^{2+}, while Ni^{2+} appears to be less electrochemically active. Also, changing the height of the white line and absorption edge slop confirms that the phase transition of the host structure is observed. (Figure 8a; Figure 9a).

Analysis of the Fourier Transform (FT) for the Extended X-ray absorption fine structure (EXAFS) spectra from the *operando* experiment (Figure 8b, d; Figure 9b, d) shows a phase transition to the disordered structure at low potentials, characterized by a decrease in amplitude for the first and second coordination shells of Ni and Fe ions. Throughout this phase transition, bond lengths undergo continuous changes: Fe–O magnitude is splitting, corresponding to the higher bond length for $Fe^{2.5+}$–O (2.058 Å, ICSDCollCode75627) and the lower length for Fe^{3+}–O (1.891 Å, ICSDCollCode75627), confirming the formation of Fe_3O_4. In this case, the Fe–Fe distances should become longer, but in fact, the Fe–Fe (Fe–Ni) distance shortens, indicating the possibility that the original distorted LDH structure can be partly retained in the initial stage. This shift is evident in the Fourier transform magnitudes of the first and second shells of Fe and Ni ions. In the Ni K-edge spectra, all FT magnitudes shift slightly to lower R values, signifying small reductions in distances between Ni–O and Ni–Ni. Upon desodiation, the material does not revert to its initial NiFe-NO_3 LDH structure. The local Ni structure remains close to the structure at the low potentials (Figure 8c), whereas the Fe ions partially return to the initial oxidation state, confirming that the initial sodiation induces irreversible changes in the structure (Figure 9c).

It should be noted that in the compound the positions of Fe and Ni ions are connected by the oxygen Ni–O–Fe. As it was already recognized, this type of connection allows the influence of Fe ions on the oxidation state of Ni ions stabilising them at Ni (II).[37] The theoretical specific capacity calculated for NiFe–NO_3 LDH as a pure conversion material with Fe and Ni as

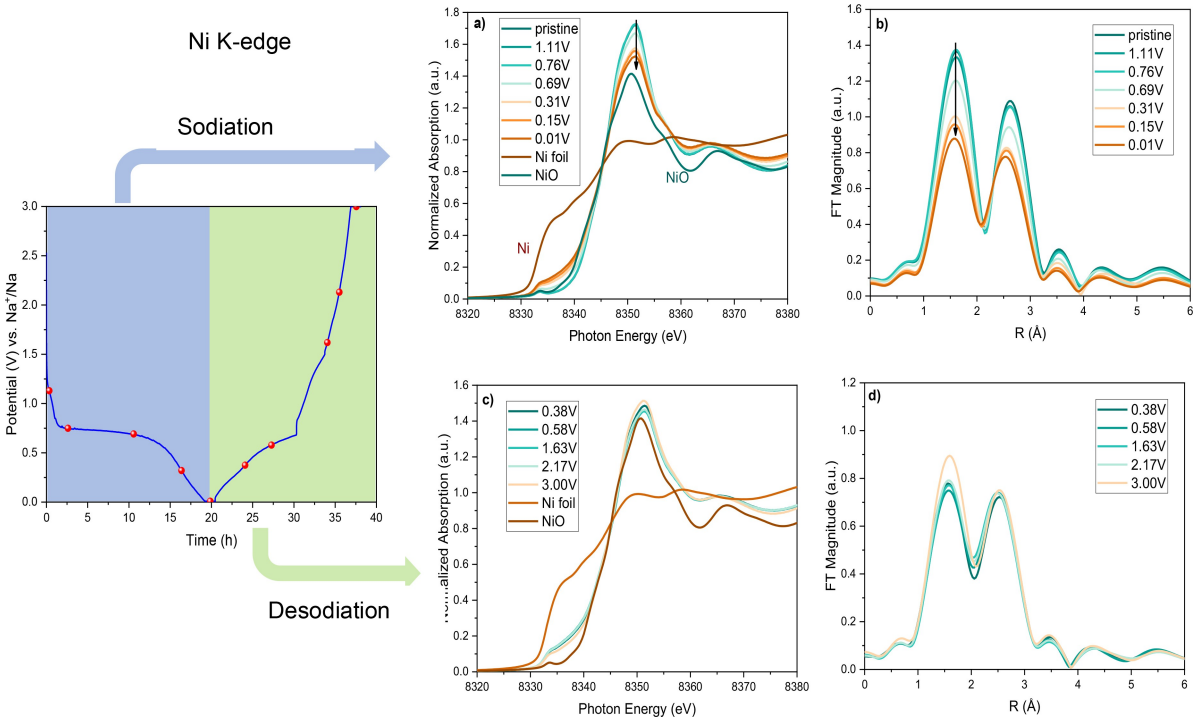

Figure 8. The normalized Ni K-edge XANES spectra (a, c) Fourier transform Ni K-edge EXAFS spectroscopy (b, d) of Ni foil, NiO standards and NiFe-NO_3 LDH.

Research Article
doi.org/10.1002/batt.202400451
Chemistry Europe
European Chemical Societies Publishing

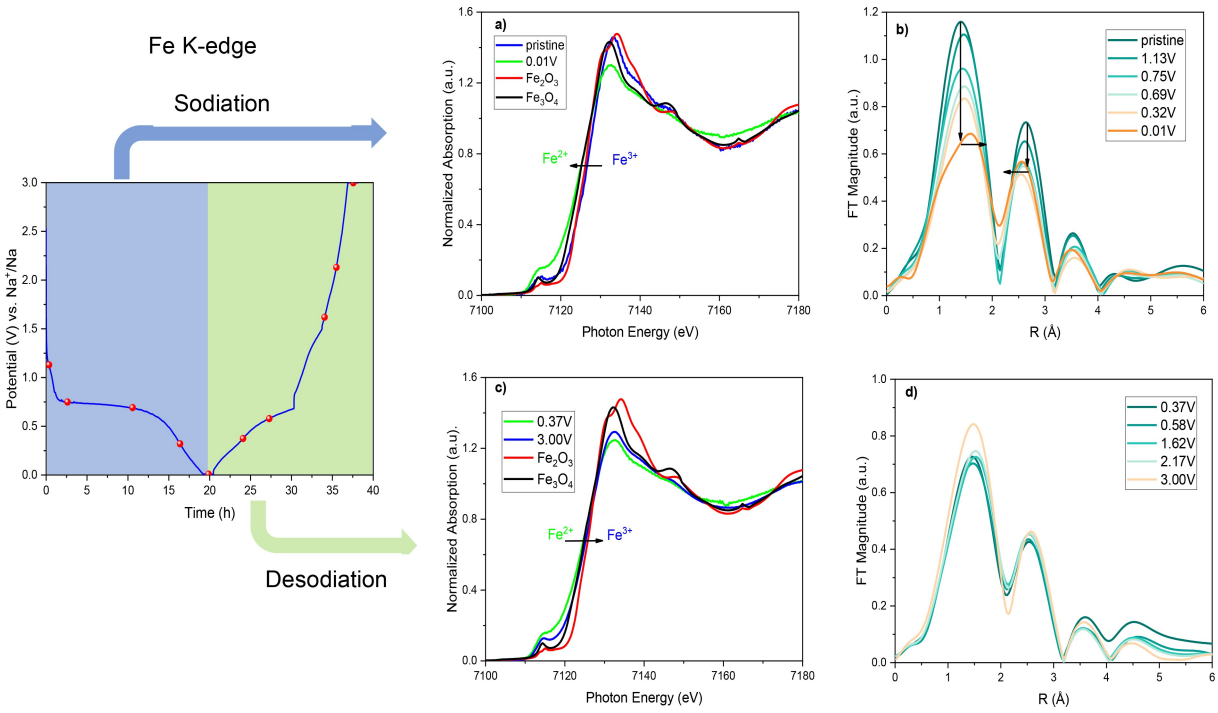

Figure 9. The normalized Fe K-edge XANES spectra (a, c) Fourier transform Fe K-edge EXAFS spectroscopy (b, d) of Fe_2O_3, Fe_3O_4 standards and NiFe-NO_3 LDH.

redox centres and assuming their reduction to the metallic state, is 477 mAh/g, this value is lower than the experimental one in first sodiation (976 mAh/g) where irreversible reactions happen (SEI formation, material irreversible modification…) but is also lower to the value in the following cycles so probably is present also a contribution of the NO_3^- that moves from the material and SEI while charging and discharging. Furthermore, from the XAS data it is demonstrated that neither Ni nor Fe reaches the (0) oxidation state so the reaction mechanism seems much more complex than expected. Considering all the previous analysis the hypothesis is that during the first sodiation a transformation of the LDH structure occurs leading to the formation of the ferrimagnetic Fe_3O_4 (partial reduction of Fe^{3+} to Fe^{2+}) and NiO_x., During desodiation those compounds undergo a reoxidation to the mixture NiO and α-Fe_2O_3 that exhibit an antiferromagnetic behaviour. The mechanism, after the first cycle, is a mixture of intercalation and conversion reactions and could be resumed in the following scheme (eq. 1, 2, 3).

By analysing the edge shift of the Ni K-edge and the Fe K-edge on the normalised μ(E) spectrum (Figure 8a, c, Figure 9a, c) together with their derivative, we can propose fist intercalation Na^+ ions to the NiFe-NO_3 LDH structure. To estimate capacity, the sodiation activity of the spinel phase Fe_3O_4 is calculated at 116 mAh/g (1 Na). The NiO oxide, unlike the spinel phase, has the probability to rebuild the LDH structure but remains less electrochemically active (179 mAh/g, 0.5 Na).[39] The presence of some other reversible reactions (involving NO_3^-) and different phases could not be excluded. FT-IR spectra confirm the decomposition of the NiFe-NO_3 LDH structure at the sodiated state with the formation of free NO_3^- ions in the electrolyte and the presence of vibrational modes for Fe_3O_4 and NiO_x for the electrode as displayed in S7. To the best of our knowledge, during the sodiation process, NiFe-NO_3 LDH can reach reduced oxide phases, while the desodiation process can produce oxidized oxide forms that may partially reconstruct the LDH structure through the memory effect.

Phase transitions :

$$NiFe-NO_3\ LDH \diamond Fe_3O_4; NiO_x \rightleftarrows NiO;\ \alpha - Fe_2O_3 \quad (1)$$

sodiation mechanism :

$$Fe_3^{+2,66}O_4 + Na^+ + e^- \rightarrow NaFe_3^{+2,33}O_4 \left(Q = 116\frac{mAh}{g}\right) \quad (2)$$

$$NiO_x + yNa^+ + ye- \rightarrow Na_yNiO_x \left(y = 0.5,\ Q = 179\frac{mAh}{g}\right) \quad (3)$$

Conclusions

It has been demonstrated that, NiFe-NO_3 LDH can be applied as an anode material for SIBs delivering in the first desodiation over 1000 mAh/g of specific capacity and stabilising around 500 mAh/g within a few cycles. This observed trend may be attributed to initial irreversible reactions that completely change the nature of the active material originating a new and more stable red-ox centre. This was demonstrated by different analysis: XAS revealed that Ni (II) in desodiation is not reduced to Ni (0), as expected at low potential, and only Fe^{3+} undergoes a complete reduction to Fe $^{2+}$. This trend is in accordance with what is present in literature, in fact, the direct oxygen bond Ni–O–Fe stabilizes the oxidation state of Ni at the expense of

Research Article
doi.org/10.1002/batt.202400451
Chemistry Europe
European Chemical Societies Publishing

Fe,[37] this mechanism mitigates the complete conversion reactions that usually is associated with a dramatic volume change preserving electrode integrity. Another crucial component that could contribute to material stability appears to be NO_3^- but further studies are needed to investigate this hypothesis. Furthermore, the theoretical specific capacity of NiFe–NO_3 LDH, considering only Ni and Fe as redox centres, is 477 mAh/g. However, experimental data surpass this value even after 50 cycles, indicating the occurrence of additional reversible reactions. Until now, the most plausible reaction mechanism is expressed in equation 1:

$$NIFe - NO_3\ LDH \rightarrow Fe_3O_4;\ NiOx \rightleftarrows NiO;\ \alpha - Fe_2O_3 \quad (1)$$

After the first sodiation, the material forms a mixture of NiOx intercalated with Na and Fe_3O_4. Subsequently, it transforms reversibly into a mixture of NiO and α-Fe_2O_3 through a combined intercalation/conversion mechanism. The material exhibits a notable initial irreversible capacity loss, rendering it currently unsuitable for large-scale applications. Further studies are required to enhance its competitiveness and suitability for widespread commercial use.

Experimental Section

Material Synthesis

The LDH was synthetised with a nickel/iron metal ratio = 2 through a simple coprecipitation method as proposed by Boclair et al.[13]

All the chemicals where of analytical grade and were purchased by Sigma-Aldrich, the deionised water (18 MΩ/cm) was boiled and purged with argon before using.

The proper amount of the metals nitrate ad sodium nitrate was solubilized in a balloon under argon atmosphere and slowly titrated with a 50% m/m solution of NaOH added with a peristaltic pump.

The balloon containing the precipitate, and its mother liquor was filled with argon and put in a hoven at 70 °C for 3 days.

The compound after was filtered, washed, dried at 60 °C and grinded in an agata mortar.

Material Characterization

PXRD patterns were collected using X'Pert MPD (Philips, Almelo, Netherland) X-ray powder diffractometers equipped with a Cu anticathode ($K\alpha 1_{Cu} = 1.5406$ Å). The indexing of the obtained diffraction data was performed in comparison with the literature and the lattice parameters of the phases were calculated using the program WinPLOTR[26].

FT-IR spectra were collected using a Spectrum 65 FT-IR Spectrometer (PerkinElmer, Waltham, MA, USA) equipped with a KBr beamsplitter and a DTGS detector by using an ATR accessory with a diamond crystal; the spectra were recorded from 4000 to 600 cm^{-1}. A ZEISS SUPRA 40 V model (FESEM) was used, where the sample was analysed by applying an acceleration voltage of 5 kV for 50 s.

Inductively coupled plasma-Optical emission spectroscopy (ICP-OES) experiments were conducted utilizing a Varian Vista PRO (Springvale, Australia) with an axially oriented configuration. The sample introduction setup included a pneumatic nebulizer of the glass concentric K-style type (Varian) connected to a glass cyclonic spray chamber (Varian). For the Field Emission Scanning Electron Microscopy (FE-SEM) the samples were observed with a ZEISS SUPRA 40 V microscope, applying an acceleration voltage of 5 kV for 50 s.

DC magnetometry measurements were performed using a Physical Property Measurement System (PPMS) DynaCool from Quantum Design, equipped with a vibrating sample magnetometry (VSM) option. The NiFe-NO_3 LDH sample material was filled into polypropylene sample capsules (P125E from Quantum Design) and attached to a brass half-tube sample holder. For pristine powder NiFe-NO_3 LDH, the magnetic moment vs. temperature was measured from 2 to 300 K at a field of 0.5 and 5 kOe, respectively, in zero-field cooled (ZFC) and field-cooled (FC) mode. From 2 to 50 K the temperature was set in 'settle mode' and from 51 to 300 K in 'sweep mode' with a heating rate of 2 K/min. A measurement of magnetic moment was performed with a temperature step size of 1 K with an averging time of 10 seconds. The raw data values were corrected for diamagnetic contribution from the atomic closed shells according to the incremental method. Magnetic moment vs. magnetic field scans were measured for the pristine powder and for the pristine, discharged, and recharged elctrodes at 2 and 300 K in FC mode as full loop measurements with a maximum magnetic field of 70 kOe. At each field two measurements were performed, each with an average time of 10 seconds. See table S1 in supporting materials for used sample masses/amounts and molar masses for magnetometry measurements.

Electrochemical Studies of Half-Cell

NiFe-NO_3 LDH electrodes have been prepared as follows: 70 mass% of the synthesised NiFe-NO_3 LDH was mixed in an agata mortar for 10 min with 20 mass% conductive carbon black (TIMCAL® Super C65) and 10 mass% of sodium alginate (SA, Sigma-Aldrich) solubilised in a 9:1 water/isopropanol solution. The blended slurries were then coated on a 10-μm-thick copper foil current collector with a wet thickness of ~150 μm dried in hoven at 60 °C. The coated electrodes were cut into individual disks of 12-mm diameter with ~1.5-mg mass loading, pressed at 8 ton and dried in an under vacuum oven at 80 °C for 12 h.

For the *in-operando* XAS analysis some electrodes where prepared in a different way: a drop of the previous mixture was deposited on a carbon foil, dried, and cut in 12 mm diameter discs than pressed at 5 ton.

Swagelock® T-cells cells were built in an argon-filled glovebox (MB200, MBraun GmbH) consisting of the as-prepared working electrode, a sodium foil counter electrode (12 mm diameter, Alfa Aesar), a glass fiber separator (Whatman glass microfiber filter, 675-μm thickness), a sodium needle control electrode (Alfa Aesar). As electrolyte was chosen a 1 M sodium perchlorate ($NaClO_4$, Alfa Aesar, >99%) solution dissolved in a mixture of 1:1 (by mass) ethylene carbonate (EC, Sigma–Aldrich, ≥99%) and dimethyl carbonate (DMC, Sigma–Aldrich, ≥99%) with a 5% (by mass) of fluoroethylene carbonate. (FEC, Sigma–Aldrich, ≥99%).

The electrochemical tests (galvanostatic cycling in potential limitation (GCPL) and cyclic voltammetry (CV)) were carried out on a multichannel potentiostat (VMP3, Bio-Logic) in the potential range (0,01-3 V vs Na^+/Na). The electrochemical cells were kept in a Binder climate chamber at 25 °C during all the experiments.

In situ XAS measurements were performed at synchrotron beamlines P64 at PETRA III (DESY), Hamburg. XAS spectra of nickel and iron were recorded in quick-XAS (6 min/spectrum) mode in

fluorescence geometry using a PIPS (passivated implanted planar silicon) diode and in transmission mode. The Ni, and Fe K- edge for LDH compounds were measured, and the energy was calibrated utilizing corresponding Ni and Fe foils as commonly applied in XAS experiments. NiO, FeO, Fe_3O_4, and Fe_2O_3 were used as standard materials, respectively. All of the data were collected at room temperature with a Si(111) double-crystal monochromator, and all of the XAS spectra were processed using the DEMETER software package.[40]

For the in-situ investigations, coin cells CR2032 (thickness = 3.2 mm) with Kapton windows (diameter = 6 mm) were used. All the electrochemical experiments were conducted using a VMP multichannel potentiostatic–galvanostatic system (Biologic Science Instrument) at room temperature, borrowed from P02.1 beamline (Dr. Martin Etter). The potential window was 0.01–3 V vs Na/Na^+ with an applied current of 30 mA/g.

Acknowledgements

This work contributes to the research performed at CELEST (Center for Electrochemical Energy Storage Ulm-Karlsruhe) and was funded by the German Research Foundation (DFG) under Project ID 390874152 (POLiS Cluster of Excellence). We acknowledge DESY (Hamburg, Germany), a member of the Helmholtz Association HGF, for the provision of experimental facilities. Parts of this research were carried out at PETRAIII and we would like to thank Dr. Aleksandr Kalinko for assistance in using beamline P64.The authors also would like to thank Dr. Liuda Mereacre for the help with FT-IR measurements and Dennis Triller for the preparation of the electrodes for FT-IR and magnetic measurements. Open Access publishing facilitated by Consiglio Nazionale delle Ricerche, as part of the Wiley - CRUI-CARE agreement.

Conflict of Interests

The authors declare no conflict of interest.

Data Availability Statement

The data that support the findings of this study are openly available in zenodo at 10.5281/zenodo.10889611, reference number 1.

Keywords: LDH · Energy storage · SIB

[1] D. Larcher, J. M. Tarascon, *Nat. Chem.* **2015**, *7*, 19–29.
[2] Z. Song, H. Zhou, *Energy Environ. Sci.* **2013**, *6*, 2280–2301.
[3] D. Kundu, E. Talaie, V. Duffort, L. F. Nazar, *Angew. Chem. Int. Ed.* **2015**, *54*, 3432–3448.
[4] S. Suriyakumar, A. Varma, V. Surendran, K. Jasuja, M. M. Shaijumon, *Batter Supercaps* **2022**, *5*, DOI 10.1002/batt.202100243.
[5] M. D. Slater, D. Kim, E. Lee, C. S. Johnson, *Adv. Funct. Mater.* **2013**, *23*, 947–958.
[6] M. He, R. Davis, D. Chartouni, M. Johnson, M. Abplanalp, P. Troendle, R. P. Suetterlin, *J. Power Sources* **2022**, *548*, 232036.
[7] M. He, A. EL Mejdoubi, D. Chartouni, M. Morcrette, P. Troendle, R. Castiglioni, *J. Power Sources* **2023**, *588*, 233741.
[8] P. Yu, W. Tang, F. F. Wu, C. Zhang, H. Y. Luo, H. Liu, Z. G. Wang, *Rare Met.* **2020**, *39*, 1019–1033.
[9] Z. L. Xu, J. Park, G. Yoon, H. Kim, K. Kang, *Small Methods* **2019**, *3*, DOI 10.1002/smtd.201800227.
[10] E. Irisarri, A. Ponrouch, M. R. Palacin, *J. Electrochem. Soc.* **2015**, *162*, A2476–A2482.
[11] D. Chaillot, S. Bennici, J. Brendlé, *Environ. Sci. Pollut. R* **2020**, DOI 10.1007/s11356-020-08498-6.
[12] F. Cavani, F. Trifirò, A. Vaccari, *Catal. Today* **1991**, *11*, 173–301.
[13] J. W. Boclair, P. S. Braterman, *Chem. Mater.* **1999**, *11*, 298–302.
[14] F. Li, X. Duan in *Applications of Layered Double Hydroxides*. Structure and Bonding, vol.119 (Eds: X. Duan, D.G. Evans) Springer, Berlin, Heidelberg. 2005 pp. 193-223 https://doi.org/10.1007/430_007.
[15] A. M. Cardinale, S. Alberti, A. Pietro Reverberi, M. Catauro, N. Ghibaudo, M. Fortunato, *Microorganisms* **2023**, *11*, 1045.
[16] T. Hu, Z. Gu, G. R. Williams, M. Strimaite, J. Zha, Z. Zhou, X. Zhang, C. Tan, R. Liang, *Chem. Soc. Rev.* **2022**, *51*, 6126–6176.
[17] A. Seijas-Da Silva, R. Sanchis-Gual, J. A. Carrasco, V. Oestreicher, G. Abellán, E. Coronado, *Batter Supercaps* **2020**, *3*, 499–509.
[18] W. Wang, D. Jiang, X. Chen, K. Xie, Y. Jiang, Y. Wang, *Appl. Surf. Sci.* **2020**, *515*, 145982.
[19] H. Zhou, F. Wu, L. Fang, J. Hu, H. Luo, T. Guan, B. S. Hu, M. Zhou, *Int. J. Hydrogen Energy* **2020**, *45*, 13080–13089.
[20] H. Liu, T. Yu, D. Su, Z. Tang, J. Zhang, Y. Liu, A. Yuan, Q. Kong, *Ceram. Int.* **2017**, *43*, 14395–14400.
[21] R. Zhang, Z. Xue, J. Qin, M. Sawangphruk, X. Zhang, R. Liu, *J. Energy Chem.* **2020**, *50*, 143–153.
[22] X. Li, M. Fortunato, A. M. Cardinale, A. Sarapulova, C. Njel, S. Dsoke, *J. Solid State Electrochem.* **2021**, DOI 10.1007/s10008-021-05011-y.
[23] M. Fortunato, A. Pietro Reverberi, B. Fabiano, A. M. Cardinale, *Energies* **2024**, *17*, DOI 10.3390/en17051035.
[24] B. Xiao, T. Rojo, X. Li, *ChemSusChem* **2019**, *12*, 133–144.
[25] P. M. Bodhankar, P. B. Sarawade, G. Singh, A. Vinu, D. S. Dhawale, *J Mater. Chem. A* **2020**, DOI 10.1039/d0ta10712c.
[26] T. Roisnel, J. Rodríquez-Carvajal, *Mater. Sci. Forum* **2001**, *378–381*, 118–123.
[27] B. Grégoire, C. Ruby, C. Carteret, *J. Chem. Soc. Dalton Trans.* **2013**, *42*, 15687–15698.
[28] M. Tian, C. Liu, Z. G. Neale, J. Zheng, D. Long, G. Cao, *ACS Appl. Mater. Interfaces* **2019**, *11*, 35977–35986.
[29] A. Maria Cardinale, M. Fortunato, F. Ardini, *Results Surf.Interfaces* **2024**, *16*, 100242.
[30] C. C. Yang, D. M. Zhang, L. Du, Q. Jiang, *J. Mater. Chem. A Mater.* **2018**, *6*, 12663–12671.
[31] D. Kong, C. Cheng, Y. Wang, Z. Huang, B. Liu, Y. Von Lim, Q. Ge, H. Y. Yang, *J. Mater. Chem. A Mater* **2017**, *5*, 9122–9131.
[32] Z. Xiao, X. Li, J. Pan, M. Qi, X. Guo, *ChemistrySelect* **2024**, *9*, e202401678.
[33] G. Abellán, J. A. Carrasco, E. Coronado, *Inorg. Chem.* **2013**, *52*, 7828–7830.
[34] S. B. Narang, K. Pubby, *J. Magn. Magn. Mater.* **2021**, *519*, 167163.
[35] R. Zysler, D. Fiorani, J. L. Dormann, A. M. Testa, *J. Magn. Magn. Mater.* **1994**, *133*, 71–73.
[36] J. C. Marmeggi, J. Baruchel, *J. Magn. Magn. Mater.* **1979**, *10*, 14–24.
[37] M. Görlin, J. Ferreira de Araújo, H. Schmies, D. Bernsmeier, S. Dresp, M. Gliech, Z. Jusys, P. Chernev, R. Kraehnert, H. Dau, P. Strasser, *J. Am. Chem. Soc.* **2017**, *139*, 2070–2082.
[38] S. Anantharaj, K. Karthick, S. Kundu, *Mater Today Energy* **2017**, *6*, 1–26.
[39] K. Lu, Y. Liu, F. Lin, I. A. Cordova, S. Gao, B. Li, B. Peng, H. Xu, J. Kaelin, D. Coliz, C. Wang, Y. Shao, Y. Cheng, *J. Am. Chem. Soc.* **2020**, *142*, 12613–12619.
[40] B. Ravel, M. Newville, *J. Synchrotron Radiat.* **2005**, *12*, 537–541.

Manuscript received: July 3, 2024
Revised manuscript received: October 31, 2024
Accepted manuscript online: December 4, 2024
Version of record online: December 17, 2024